Nuclear Instruments and Methods in Physics Research A 608 (2009) 125–131

Contents lists available at ScienceDirect

Nuclear Instruments and Methods in Physics Research A

journal homepage: www.elsevier.com/locate/nima

Microstructured semiconductor neutron detectors

D.S. McGregor *, W.J. McNeil, S.L. Bellinger, T.C. Unruh, J.K. Shultis

S.M.A.R.T. Laboratory, Department of Mechanical and Nuclear Engineering, 3002 Rathbone Hall, Kansas State University, Manhattan, KS 66506-2503, USA

ARTICLE INFO

Article history:
Received 1 April 2009
Accepted 12 June 2009
Available online 21 June 2009

Keywords:
Semiconductor neutron detectors
Solid state neutron detectors

ABSTRACT

Perforated semiconductor neutron detectors are compact diode detectors that operate at low power and can be fashioned to have high thermal neutron detection efficiency. Fabricated from high-purity Si wafers, the perforations are etched into the diode surface with ICP-RIE and backfilled with ^{6}LiF neutron reactive material. The intrinsic thermal neutron detection efficiency depends upon many factors, including the perforation geometry, size, and depth. Devices were fabricated from high resistivity 10 kΩ cm n-type Si with conformal p-type shallow junction diffusions into the perforations, which demonstrate improved neutron detection performance over previous selectively diffused designs. A comparison was made to previous selectively diffused designs, and pulse height spectra show improved signal-to-noise ratio, higher neutron counting efficiency, and excellent gamma-ray discrimination. Devices with 20 (average) μm wide 100 μm deep sinusoidal trenches yielded intrinsic thermal neutron detection efficiencies of 11.94 ± 0.078%.

1. Introduction

Semiconductor neutron detectors based on thin-film coatings of neutron reactive material (or "converter foils") in close proximity to semiconductor diodes have long been of interest. Early devices dating back several decades were fabricated from Si and SiC, usually with either ^{10}B, ^{6}LiF or a form of Gd acting as the neutron reactive material (see Refs. [1–4] for examples). Typically, the neutron reactive material is applied directly to the semiconductor to increase efficiency and decrease energy attenuation of the reaction products. Although there are several neutron reactions and reactive materials that have been used for thin-film-coated detectors, the most often quoted are the $^{10}B(n,\alpha)^{7}Li$ reaction, the $^{6}Li(n,t)^{4}He$ reaction in the form of ^{6}LiF, and the $^{157}Gd(n,\gamma)^{158}Gd$ reaction typically in the form of natural Gd due to the high cost of isotopically pure ^{157}Gd.

In the present work, the neutron reactive coating used is ^{6}LiF. ^{6}Li has a relatively large microscopic 2200 m s^{-1} neutron absorption cross section of 940 b, although it is less than those for ^{157}Gd and ^{10}B. The macroscopic 2200 m s^{-1} neutron cross section of ^{6}LiF is 57.51 cm^{-1} with a mass density of 2.54 g cm^{-3}. When thermal neutrons are absorbed in ^{6}Li, a 2.73 MeV triton and a 2.05 MeV alpha particle are ejected in opposite directions. The reaction products from the $^{6}Li(n,t)^{4}He$ reaction are more energetic than those of the $^{10}B(n,\alpha)^{7}Li$ or $^{157}Gd(n,\gamma)^{158}Gd$ reactions and, hence, are much easier to detect and discriminate from background radiations.

A detailed analysis of coated semiconductor device configurations indicates that semiconductors coated with either ^{6}LiF or ^{10}B will be limited to no more than approximately 4.5% intrinsic thermal neutron detector efficiency ε_{tn} [5]. It was suggested by Muminov that the incorporation of channels in a semiconductor substrate subsequently backfilled with a neutron reactive material might increase the thermal neutron detection efficiency of a semiconductor based diode [6], and again much later by Schelten [7,8], yet neither group built or reported working devices. Muminov [6] suggested that the extended surface area of the shallow channels will increase the overall detection efficiency, which is only partially true. It is actually both the extended surface area and the increased probability that reaction products can enter into the semiconductor material, due to additional geometric effects, that truly increases the efficiency, as pointed out elsewhere [9–11].

The first demonstration of a microstructured semiconductor neutron detector was reported by McGregor et al. [12,13]. The devices were constructed from bulk GaAs with circular hole perforations backfilled with ^{10}B [13]. Since then, microstructured semiconductor neutron detectors, also referred to as perforated neutron detectors, have been pursued with deeper channels and various geometries [9–11,14–27].

Deep microscopic structures etched into the semiconductor substrate backfilled with neutron reactive material permits higher neutron detection efficiency than common thin-film-coated planar devices [9,10]. An independent study seemed to render similar results [24]. Device geometries with different shapes and

* Corresponding author. Fax: +1 785 532 4093.
E-mail address: mcgregor@ksu.edu (D.S. McGregor).
URL: http://www.mne.ksu.edu/research/centers/SMARTlab (D.S. McGregor).

0168-9002/$ - see front matter © 2009 Elsevier B.V. All rights reserved.
doi:10.1016/j.nima.2009.06.031

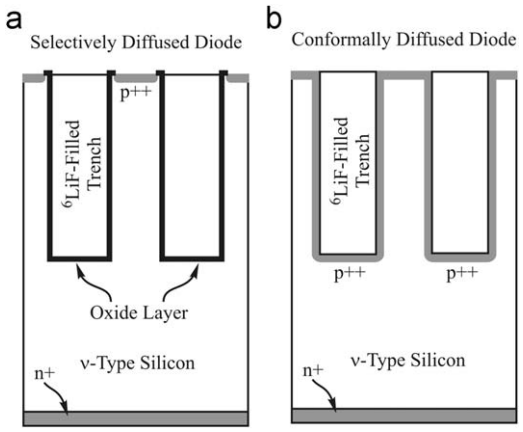

Fig. 1. Cross-sectional view of the selectively diffused perforated diode structure with side-wall passivation (a) and the conformal-diffused perforated diode structure (b).

depths were analyzed [11], and it was determined that a trench design delivers both high efficiency and performance stability as a function of the lower level discriminator (LLD) setting.

Other designs considered, "circular holes" or "pillars", were less interesting either from the standpoint of stability or efficiency [11]. Microstructured designs using circular holes tended to show increased stability in performance as a function of the LLD setting, thereby offering larger signal-to-noise ratios, yet generally deliver lower efficiencies. Microstructured designs using pillars generally indicated improved efficiency provided that the structural features were very small and the LLD was set very low. Unfortunately, pillar designs showed large changes in efficiency as a function of the LLD setting, hence are less stable. By contrast, the trench and circular hole designs were much more robust [11].

Advanced trench designs have been investigated to (1) increase structural integrity and (2) increase uniformity in response to varying incident neutron directions [17,19,23]. The designs consist of either chevron or sinusoidal shaped trenches, and deliver high efficiencies similar to straight trench designs [17], while performing with improved uniformity of response with respect to irradiation direction [19]. Microstructured patterns based on a matrix of holes, pillars or straight trenches will have streaming pathways where neutrons can pass without intersecting the absorber material, even with stacked devices. The chevron and sinusoidal designs help to suppress neutron streaming paths through the detector, thereby providing a more uniform directional response to neutrons [17]. The relative efficiencies of these sinusoidal devices, as compared to planar thin-film-coated detectors and common ^{3}He gas-filled detectors, show great promise.

Several process designs have been proposed for the fabrication of microstructured semiconductor detectors, which include the selectively diffused design and the conformally diffused design [18,23]. In the present work, using the sinusoidal microstructured design, performance comparisons between selectively diffused and conformally diffused structures are shown (See Fig. 1). Absolute thermal neutron detection efficiencies are reported, and comparisons to theoretical predictions are made.

2. Modeling results

Device modeling has been used to determine the best pattern for neutron detection efficiency and efficiency stability as a function of the LLD, and the reader is referred to Ref. [11] for details. For trench-type designs, which include sinusoids and chevrons, the cavities are referred to as trenches and the semiconductor material between the trenches are called fins. The modeling included a Monte Carlo approach to determine the expected spectral features as a function of the trench depth and width, and also the semiconductor fin width [11]. Shown in Fig. 2 are the expected spectral features for a ^{6}LiF backfilled Si device with 90 μm deep trenches, showing the features for 12.5, 18.75, and 25 μm trench and fin widths, based on energy deposition. There are a few features that become readily apparent, those being the wide "valley" in the low energy region (from 0 to approximately 0.8 MeV), a peak area in the central portion of the spectrum, and a tail region extending into the higher energy region. The reason these features appear is explained elsewhere [11].

The fortuitous consequences of the valley region at low energies are a reduction in the dependence of the thermal neutron detection efficiency ε_{tn} on the LLD setting, and an improved gamma-ray rejection ratio since the LLD can be set selectively high. Shown in Fig. 3 are the modeled thermal neutron detection efficiencies for ^{6}LiF backfilled trench devices for the cases in which the trench and fin widths are either 12.5, 18.75, or 25 μm, all of which are 90 μm deep. Notice that the change in efficiency is small between an LLD setting of 0 up to approximately 0.7 MeV. For instance, a device with 12.5 μm wide trench reduces only from 16.76% to 15.4% ε_{tn} when the LLD is raised from 0 to 0.7 MeV. Since there are fewer counts recorded in the region between 0 and 0.7 MeV than in the higher energy region (above 0.7 MeV), then increasing the LLD through the lower energy region has little effect on ε_{tn}. As shown in Fig. 3, the expected ε_{tn} values for 90 μm deep ^{6}LiF backfilled trenches with trench and fins widths between 12.5 and 25 μm range between 11% and 17% for LLD settings between 0 and 0.7 MeV.

3. Detector development

There are efforts from other groups to manufacture various microstructured patterns [24,26], both of which show increased noise in spectra taken with etched semiconductor microstructures with small dimensions on the order of tens of microns, as also witnessed by the authors [15], and determined to be, at least in part, due to surface damage along the microstructure sidewalls. As a result, the LLD must be increased well above the noise level to reduce dead time resulting from electronic noise and leakage currents, a necessity which unfortunately decreases ε_{tn} [11]. Two approaches were taken to reduce leakage current in the basic design, including selectively diffusing p-type dopants between the trenches and growing a thermal oxide inside the trenches to increase the surface resistance (as depicted in Fig. 1(a)) [15,27], thus, slightly complicating the fabrication process [19,27]. Yet, the pulse height spectra from these selectively diffused devices do not match the basic modeled characteristics shown in Fig. 3 (and detailed in [25]); hence it is possible that surface damage caused from the processing steps, inadvertent doping, or perhaps other processing complications have prevented full depletion of the device while still causing some spectral contamination from electronic noise.

An alternative method for making the microstructured semiconductor neutron detectors requires diffusing the pn junction inside the trench structure [18]. The diode contact geometry is no longer produced on the primary pre-etched surface, but conforms to the surface of the trench structure as shown in Fig. 1(b). This fabrication method consumes etch damage in the perforation, hence, is not affected by the etched surface and does not require the oxide passivation step.

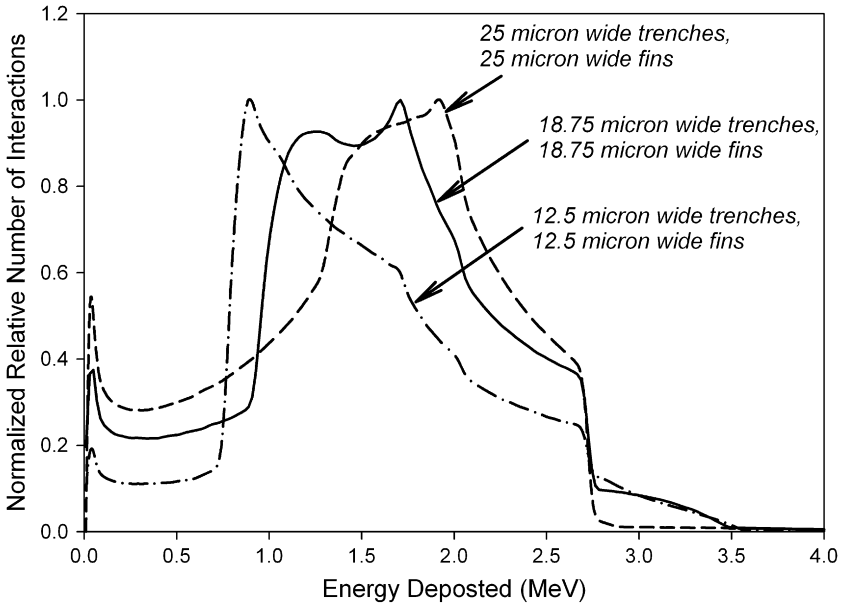

Fig. 2. Modeled spectra for 90 μm deep ^{6}LiF backfilled trench devices for the cases in which the trench and fin widths are either 12.5, 18.75, or 25 μm wide. The spectra are normalized to the highest point of each spectrum and show the relative normalized number of events per unit energy deposited.

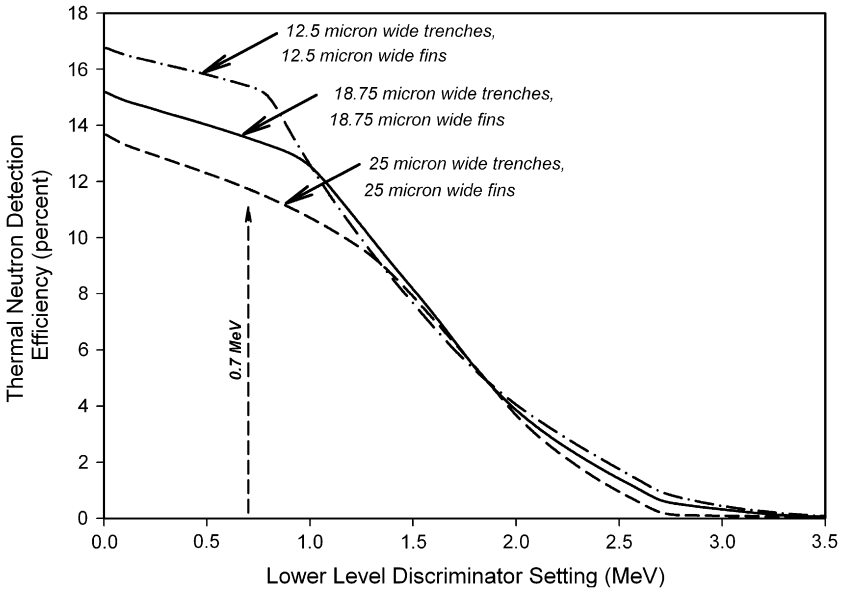

Fig. 3. Modeled thermal neutron detection efficiencies for 90 μm deep ^{6}LiF backfilled trench devices for the cases in which the trench and fin widths are either 12.5, 18.75, or 25 μm.

The perforations are etched with ICP-RIE into float zone refined 10 kΩ n-type (or ν-type) Si. The detector active area is 6 mm in diameter, and are batch processed on 3-in. diameter wafers. The devices reported in the present work have etched sinusoidal perforations ranging between 20 and 26 μm wide and 100 μm deep (see Fig. 4 and also Ref. [17]). The sinusoidal design eliminates the angular dependence on sensitivity resulting from neutron streaming [17,19,27], thereby, increasing the intrinsic thermal neutron detection efficiency while producing a flat detection response throughout a wide solid angle around normal incidence [17,19,27]. Figs. 5 and 6 show the microstructure of the sinusoidal perforated device.

After the etch process, the surface is patterned with photoresist and p-type regions are diffused uniformly into the device structure, thereby forming pn junctions within the trenches. Afterwards, a single Ti–Al metal contact ring is fabricated around the detector perimeter to make electrical contact to the p-type region. The back surface is coated with a metal contact to complete the diode structure. Finally, ^{6}LiF powder is packed into the perforations to perform as the neutron absorbing converter layer material (Fig. 7). Neutrons that interact in the ^{6}Li spontaneously emit 2.05 MeV alpha particles and 2.73 MeV tritons, which then enter the semiconductor material and are subsequently detected in the perforated Si diode.

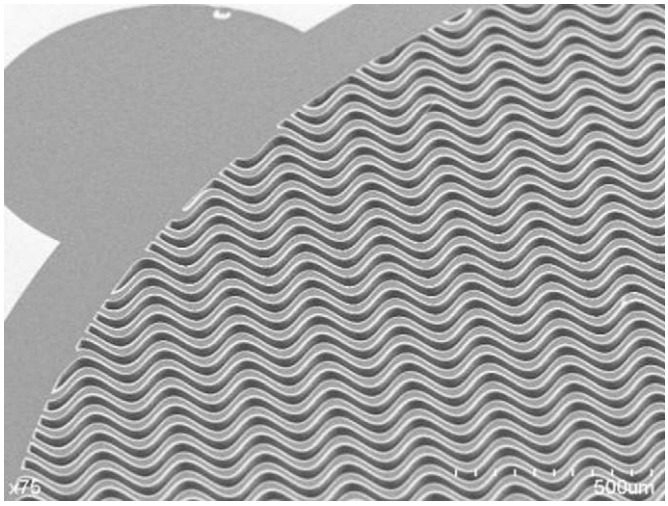

Fig. 4. Streaming effects are eliminated by using sinusoidal perforation patterns. The pattern increases the intrinsic thermal neutron detection efficiency while producing a uniform detection response. The channels are later backfilled with ^{6}LiF powder. The rounded semi-circle in the upper left is the detector bonding pad.

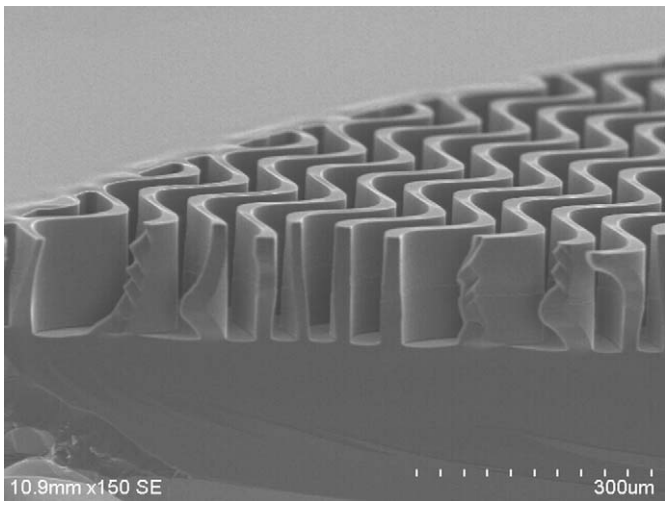

Fig. 5. Microstructure of the perforated patterns etched into a Si substrate, showing detail of the sinusoidal pattern.

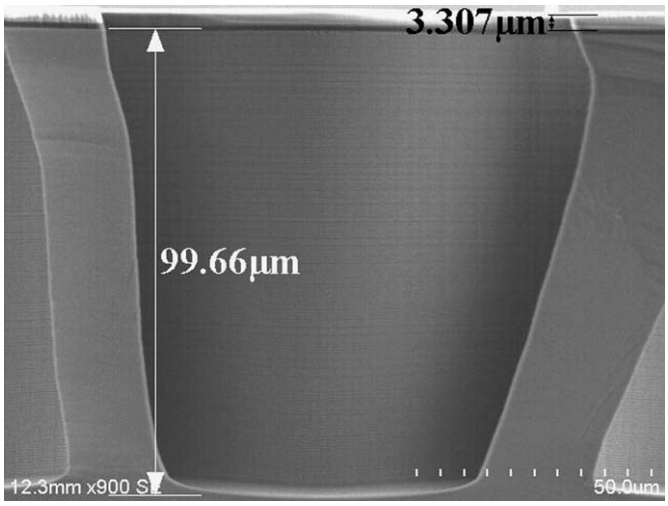

Fig. 6. Microstructure of the perforated patterns etched into a Si substrate, showing the height and detail of a single perforation.

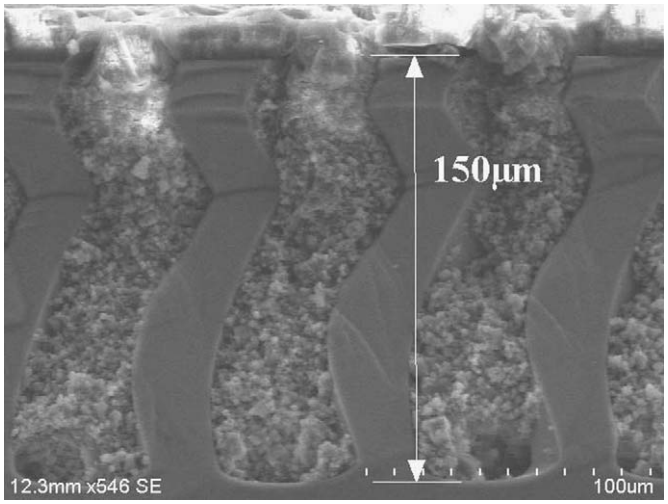

Fig. 7. Cross-section detail of 150 µm deep ^{6}LiF backfilled sinusoidal trenches. Note that the apparent curves in the Si semiconductor result from an oblique angle cleave to the wafer surface.

4. Calibration of detectors

Previous works reported relative efficiencies as compared to a ^{3}He gas-filled detector, which served to demonstrate the validity of the perforated detector concept [19]. Because ^{3}He gas-filled detectors often have insensitive regions at the ends and can also have non-uniform absorption from the sides, the absolute efficiency of the ^{3}He gas-filled detector was unknown. In the present work, calibrated standard thin-film-coated neutron detectors were used to determine the neutron flux, which included ^{10}B-coated and ^{6}LiF-coated Si diodes. A comparison was then made to a standard ^{3}He gas-filled detector which was used as an additional check to determine the absolute value of ε_{tn} for the perforated detectors, thereby, permitting direct comparisons of the measured intrinsic efficiencies to calculated results.

A diffracted neutron beam from the Kansas State University TRIGA Mark II nuclear reactor was used for the efficiency calibrations. The beam diffraction angle was set to yield 0.0253-eV thermalized neutrons to the work space. The neutron beam was stopped down to a diameter of 1.27 cm with a cadmium shutter. The ^{3}He detector used was a 2-in. diameter, 6-in. long Reuter Stokes model P4-1603-207. The device has a 35-mil thick (889 µm) 304-stainless-steel shell, which can absorb 10% or more of the neutron beam.

Because the ^{3}He detector has long field tubes inside at each end, there are appreciable dead regions at each end of the detector. The ^{3}He detector was laid sideways and centered in the neutron beam, such that the beam intersected perpendicular to the axis of the detector (not along the long axis), to measure the relative attenuation of the beam as it passed through the tube. The total transmission of the neutron beam as it passes through two walls of stainless steel and the ^{3}He gas is

$$I_{out} = I_{in} e^{-2\Sigma_s t_s} e^{-\Sigma_{He} t_{He}} \tag{1}$$

where I_{in} is the neutron count rate before attenuation through the ^{3}He detector, I_{out} is the neutron count rate after attenuation through the ^{3}He detector, Σ_s is the macroscopic cross section of the ^{3}He detector stainless-steel tube, Σ_{He} is the macroscopic cross section of the ^{3}He gas, t_s is the thickness of the ^{3}He detector stainless-steel tube, and t_{He} is the inner diameter of the ^{3}He gas detector. A BF_3 neutron detector was placed behind the ^{3}He

detector to measure the transmission factor

$$T_d = e^{-2\Sigma_s t_s} e^{-\sigma_{He} t_{He}} = \frac{I_{out}}{I_{in}}. \quad (2)$$

Hence, T_d yields the attenuation through both the stainless-steel shell and the ^{3}He gas of the ^{3}He gas detector. With the assumption that 2 in. of air has little effect on the neutron beam attenuation, the steel shell transmission factor was determined by placing an empty 304-stainless-steel tube casing, with the same steel-thickness and radius of the ^{3}He gas detector, in the beam, and measuring the transmission factor

$$T_{2s} = e^{-2\Sigma_s t_s} = \frac{I_s}{I_{in}} \quad (3)$$

where I_s is the count rate from the beam attenuated by the empty stainless-steel-tube casing. It is assumed that the gas of the ^{3}He detector is the sensitive volume and attenuation in the gas accounts for all neutron counts produced by the detector. Conversely, it is also assumed that any additional attenuation in the steel casing does not contribute to counts. The transmission factor of the detector gas is determined by substituting Eq. (3) into (2) to yield

$$T_g = \frac{I_{out}}{I_s} = e^{-\Sigma_{He} t_{He}}. \quad (4)$$

The fraction of the beam attenuated by the gas in the detector reveals the fraction of interactions in the ^{3}He, yet it does not yield directly the detector efficiency. The beam that is attenuated in the ^{3}He gas was already attenuated by a single thickness of the steel casing. Hence, the fraction of the beam that is transmitted through one thickness of the sheet metal is

$$T_{1s} = e^{-\Sigma_s t_s} = [e^{-2\Sigma_s t_s}]^{1/2} = \left[\frac{I_s}{I_{in}}\right]^{1/2}. \quad (5)$$

Noting that the efficiency is determined by neutrons absorbed in the ^{3}He gas, the ^{3}He detector efficiency is determined by combining Eqs. (4) and (5)

$$\varepsilon_{He} = e^{-\Sigma_s t_s}(1 - e^{-\Sigma_{He} t_{He}}) = \left[\frac{I_s}{I_{in}}\right]^{1/2}\left(1 - \frac{I_{out}}{I_s}\right). \quad (6)$$

All measurements for the calibration were performed for identical times Δt, with $I_{in}\Delta t = 22952$, $I_{out}\Delta t = 2089$, and $I_s\Delta t = 18891$. With application of error propagation to Eq. (6), the measurements yielded an intrinsic efficiency for 0.0253 eV neutrons in a stopped-down neutron beam (1.27-cm diameter) passing sideways through the center of the ^{3}He detector as 0.807 ± 0.005 or $80.7 \pm 0.50\%$. The ^{3}He gas-filled detector was then used to calibrate the diffracted neutron intensity, yielding $I = 291 \pm 1.8\,\mathrm{n\,cm^{-2}\,s^{-1}}$ at a reactor power level of 2 kW.

With the calibrated efficiency of the ^{3}He detector, several planar coated diodes were tested, and their efficiencies were compared to the theoretical efficiency values. The planar detectors had coatings of ≈ 450 Å ^{10}B, 18 μm ^{6}LiF, and 27 μm ^{6}LiF, individually. To isolate the alpha particle contribution to the spectrum for the device coated with ≈ 450 Å of ^{10}B, the LLD was set to 1100 keV equivalent during operation, yielding a measured efficiency of $0.101 \pm 0.0006\%$ with an expected efficiency of 0.116% [5]. The device coated with 18 μm of ^{6}LiF was operated with an LLD setting of 300 keV, and the measured efficiency was $3.75 \pm 0.034\%$ with an expected efficiency of 3.99% [5]. The device coated with 27 μm of ^{6}LiF was operated with an LLD setting of 380 keV, and the measured efficiency was $4.19 \pm 0.032\%$ with an expected efficiency of 4.3% [5]. Overall, the efficiencies measured from the neutron beam as calibrated from the ^{3}He gas-filled detector matched well to theoretical values, hence providing validation for the neutron beam flux measurement.

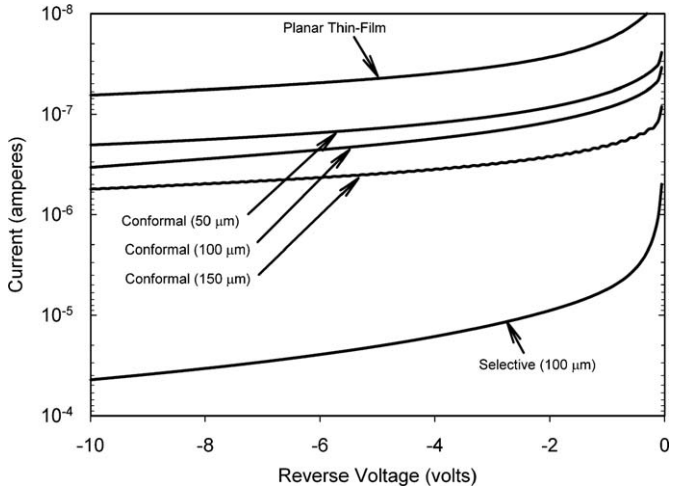

Fig. 8. Leakage current from a planar thin-film-coated detector, a selective-diffused diode with 100 μm deep trenches, and three conformal-diffused diodes with 50, 100, and 150 μm deep trenches. All devices were 6 mm in diameter.

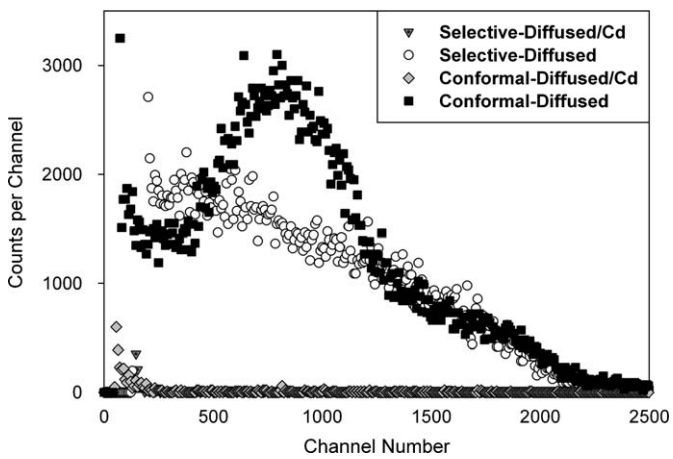

Fig. 9. Typical spectra from selective-diffused and conformal-diffused diode detectors with 100 μm deep sinusoidal perforations, showing response with and without (Cd shuttered) neutrons.

5. Performance of sinusoidal perforated detectors

Detectors with selectively diffused regions around the perforations suffer nearly two orders of magnitude greater leakage current than the conformally diffused perforated diodes as shown in Fig. 8. Although the conformally diffused detector leakage current is slightly higher than that observed for a simple planar diode, the neutron detection performance increase is superior to both the simple planar and selectively diffused detectors. During all neutron detection measurements, the conformally diffused device was operated at 5 V reverse bias and the selectively diffused detector was operated at 3 V reverse bias. The selectively diffused device was operated at a lower voltage because of its higher leakage current.

A comparison of pulse height spectra from a selectively diffused perforated neutron detector (Fig. 1(a)) and a conformally diffused perforated neutron detector (Fig. 1(b)) is shown in Fig. 9. Both detectors have a sinusoidal pattern etched 100 μm deep. Prompt gamma rays emitted from the thin Cd shutter appeared in the spectrum as numerous pulses at low energy channels near the

detector system noise levels (Fig. 9). It is clear that the selectively diffused perforated device produces an entirely different spectrum from that of the selective-diffused device, and closely resembles the calculated spectra shown in Fig. 2 and published elsewhere [25]. A broad peak is formed by the conformally diffused device in its pulse height spectrum with a sizeable gap between the gamma-ray pulses at the lower energy portion of the spectrum, as predicted [25]. Note that the main features expected from the calculated results shown in Fig. 2 appear in the conformally diffused spectrum, but not in the selectivelydiffused spectrum. Hence, it is believed that the reaction product energy deposition in the active region of the conformally diffused device mimics the expected results from the idealized model, in which the model was based on the assumption that the entire region surrounding the cavities is active. Also, the modeled results seem to indicate that the selectively diffused device is not fully depleted around the cavities, hence some of the reaction product energy absorbed in the detector does not contribute to the signal.

The calibration of neutron counting efficiency was performed with the LLD set at channel 200 (approximately equivalent to 300 keV) for both detectors (see Fig. 9) to eliminate gamma-ray background counts. The value of ε_{tn} was calculated by dividing the total neutron counts collected from the detector by the neutron fluence determined from the neutron flux measured with the calibrated standard ^{3}He detector. The resulting values of ε_{tn} were $8.96 \pm 0.059\%$ and $11.94 \pm 0.078\%$ for the selectively diffused design and the conformally diffused design, respectively. The conformally diffused diode detector is collecting more neutron counts for the same size of device and perforation depths than the selectively diffused device. The improvement provides more evidence for an increased depletion depth and larger active region in the conformally diffused device over that of the selective-diffused device [27].

The conformally diffused detector was independently tested with a 4.62 μCi ^{60}Co source to determine the gamma-ray detection efficiency. The gamma-ray source was place exactly 1 cm away from the detector and a counting spectrum was taken. A background count was also taken to subtract any background counts and noise contributions. The gamma-ray detection efficiency was determined by dividing the source fluence into the integrated counts in the spectrum. These results were then compared to the thermal neutron detection efficiency measured for the conformally diffused neutron detector. With the LLD set at 200 keV, the gamma-ray rejection ratio was determined to be greater than 3×10^{6} neutrons per gamma ray, and with the LLD set to 500 keV the gamma-ray rejection ratio is greater than 1.6×10^{7} neutrons per gamma ray.

6. Conclusions

Overall, the conformally diffused diode design appears to be a superior design for perforated neutron detectors when compared to the various selectively diffused diode structures [19,27]. The measured efficiency of the conformally diffused sinusoidal microstructured detectors, with the LLD set at approximately 300 keV, matches well to the predicted ε_{tn} values for detectors. The calculated efficiencies for 100 μm deep microstructured trench detectors with 18.75 and 25 μm wide trenches, also with the LLD set at 300 keV, are ε_{tn} of 12.8% and 14.45%, respectively. Estimating an average ε_{tn} of 13.65%, the value of $11.94 \pm 0.078\%$ falls approximately 12.5% below the predicted value. The measured reduced efficiency can be easily explained as a consequence of the ^{6}LiF powder packing fraction, in which the effective density is reduced (by approximately 15%) due to space between the ^{6}LiF granules. Note, however, that the reaction product ranges will actually increase as a result of the lower density of ^{6}LiF. Further, the leakage currents for the conformally diffused microstructured detectors are considerably lower than the leakage currents observed for selective-diffused microstructured detectors. Finally, the gamma-ray rejection ratio was found to be greater than 3×10^{6} neutrons per gamma ray with the LLD set at 200 keV. The reason for the high gamma-ray rejection ratio results from combined effects, as explained elsewhere [11]. Future conformally diffused devices will incorporate deeper trench designs along with stacked devices, as also described elsewhere [18,23].

Calculations indicate that Si detectors with 12.5 μm wide trenches and semiconductor fins, at depths of 175 μm backfilled with ^{6}LiF, can deliver ε_{tn} values exceeding 25% [11]. Appropriately stacking two such devices can, therefore, provide a total ε_{tn} exceeding 50%. For a single detector design, ε_{tn} values exceeding 34% can be fabricated for devices with 14 μm wide trenches and 6 μm wide semiconductor fins, all being 175 μm deep backfilled with ^{6}LiF [11]. Although these smaller microstructure geometries are certainly more challenging to fabricate than the microstructure geometries presented in the present work, they are not impossible to produce. Future work will be dedicated to the fabrication and testing of these aggressive microstructure designs, with the goal of reaching 50% ε_{tn}, a goal that is easier to accomplish with the newer conformally diffused detector design.

Acknowledgments

This work was supported in part by DRTA Contract DTRA-01-03-C-0051, NSF Grant no. 0412208, and DOE Grant no. DE-FG07-04ID14599.

References

[1] R.V. Babcock, R.E. Davis, S.L. Ruby, K.H. Sun, E.D. Wolley, Nucleonics 17 (1959) 116.
[2] B. Feigl, H. Rauch, Nucl. Instr. and Meth. 61 (1968) 349.
[3] A. Rose, Nucl. Instr. and Meth. 52 (1967) 166.
[4] Biographical Series no. 18, Neutron Detectors, IAEA, Vienna, 1966 (references therein).
[5] D.S. McGregor, M.D. Hammig, Y.-H. Yang, H.K. Gersch, R.T. Klann, Nucl. Instr. and Meth. A 500 (2003) 272.
[6] R.A. Muminov, L.D. Tsvang, Sov. At. Energy 62 (1987) 255.
[7] J. Schelten, M. Balzhäuser, F. Höngesberg, R. Engels, R. Reinartz, Physica B (1997) 1084.
[8] J. Schelten, R. Reinartz, Neutron detector, US Patent 58804762, allowed March 9, 1999.
[9] J.K. Shultis, D.S. McGregor, in: Conference Record IEEE Nuclear Science Symposium, Rome, Italy, October 18–22, 2004, p. 4569.
[10] J.K. Shultis, D.S. McGregor, IEEE Trans. Nucl. Sci. NS-53 (2006) 1659.
[11] J.K. Shultis, D.S. McGregor, Nucl. Instr. and Meth. A 606 (2009) 608.
[12] D.S. McGregor, R.T. Klann, H.K. Gersch, E. Ariesanti, J.D. Sanders, B. VanDerElzen, in: Conference Record IEEE Nuclear Sciences Symposium, San Diego, California, November 4–9, 2001, p. 2401.
[13] D.S. McGregor, R.T. Klann, H.K. Gersch, E. Ariesanti, J.D. Sanders, B. VanDerElzen, IEEE Trans. Nucl. Sci. NS-49 (2002) 1999.
[14] D.S. McGregor, R.T. Klann, Pocked surface neutron detector, US Patent 6545281, allowed April 8, 2003.
[15] W.J. McNeil, S. Bellinger, T. Unruh, E. Patterson, A. Egley, D. Bruno, M. Elazegui, A. Streit, D.S. McGregor, in: Conference Record IEEE Nuclear Sciences Symposium, San Diego, CA, October 29–November 3, 2006, p. 3732.
[16] D.S. McGregor, S. Bellinger, D. Bruno, W.L. Dunn, W.J. McNeil, E. Patterson, B.B. Rice, J.K. Shultis, T. Unruh, Radia. Phys. Chem. 2009, in press.
[17] C.J. Solomon, J.K. Shultis, W.J. McNeil, B.B. Rice, D.S. McGregor, Nucl. Instr. and Meth. A 580 (2007) 326.
[18] D.S. McGregor, R.T. Klann, High-efficiency neutron detectors and methods of making the same, US Patent 7164138, allowed January 16, 2007.
[19] S.L. Bellinger, W.J. McNeil, T.C. Unruh, D.S. McGregor, in: IEEE Nuclear Sciences Symposium, Waikiki, Hawaii, October 28–November 3, 2007, p. 1904.
[20] D.S. McGregor, S.L. Bellinger, D. Bruno, W.J. McNeil, E. Patterson, J.K. Shultis, C.J. Solomon, T. Unruh, Proc. SPIE 6706 (2007) 0N1.
[21] D.S. McGregor S. Bellinger, D. Bruno, W.J. McNeil, E. Patterson, B.B. Rice, in: Proceedings of 32nd Annual GOMACTech Conference, Lake Buena Vista, FL, March 19–22, 2007.

[22] Q. Jahan, E. Patterson, B. Rice, W.L. Dunn, D.S. McGregor, Nucl. Instr. and Meth. B 263 (2007) 183.
[23] D.S. McGregor, S.L. Bellinger, W.J. McNeil, E.L. Patterson, B.B. Rice, J.K. Shultis, C.J. Solomon, US-patent pending, filed March 14, 2007.
[24] J. Uher, F. Frojdh, J. Jakubek, C. Kenney, Z. Kohout, V. Linhart, S. Parker, S. Petersson, S. Pospisil, G. Thungstrom, Nucl. Instr. Meth. A 576 (2007) 32.
[25] D.S. McGregor, J.K. Shultis, Proc. SPIE 7079 (2008) 0601.
[26] R.J. Nikolic, A.M. Conway, C.E. Reinhardt, R.T. Graff, T.F. Wang, N. Deo, C.L. Cheung, Appl. Phys. Lett. 93 (2008) 133502.
[27] S.L. Bellinger, W.J. McNeil, T.C. Unruh, D.S. McGregor, IEEE Trans. Nucl. Sci. 56 (2009) 742.